BJR

https://doi.org/10.1259/bjr.20170605

Received: 17 August 2017 | Revised: 30 January 2018 | Accepted: 13 February 2018

Cite this article as:
Deng C-Y, Juan Y-H, Cheung Y-C, Lin Y-C, Lo Y-F, Lin GG, et al. Quantitative analysis of enhanced malignant and benign lesions on contrast-enhanced spectral mammography. *Br J Radiol* 2018; **91**: 20170605.

FULL PAPER

Quantitative analysis of enhanced malignant and benign lesions on contrast-enhanced spectral mammography

[1]CHIH-YING DENG, MD, [1,2]YU-HSIANG JUAN, MD, [1,2]YUN-CHUNG CHEUNG, MD, [1,2]YU-CHING LIN, MD, [3]YUNG-FENG LO, MD, PhD, [1,2]GIGIN LIN, MD, PhD, [2,3]SHIN-CHEH CHEN, MD and [1,2]SHU-HANG NG, MD

[1]Department of Medical Imaging and Intervention, Chang Gung Memorial Hospital, Linkuo and Taoyuan, Taiwan
[2]Department of Medical Imaging and Radiological Sciences, Medical College of Chang Gung University, Taoyuan, Taiwan
[3]Department of Surgery, Chang Gung Memorial Hospital at Linkou, Taoyuan, Taiwan

Address correspondence to: Dr Yun-Chung Cheung
E-mail: *alex2143@cgmh.org.tw*

Objective: To retrospectively analyze the quantitative measurement and kinetic enhancement among pathologically proven benign and malignant lesions using contrast-enhanced spectral mammography (CESM).
Methods: We investigated the differences in enhancement between 44 benign and 108 malignant breast lesions in CESM, quantifying the extent of enhancements and the relative enhancements between early (between 2–3 min after contrast medium injection) and late (3–6 min) phases.
Results: The enhancement was statistically stronger in malignancies compared to benign lesions, with good performance by the receiver operating characteristic curve [0.877, 95% confidence interval (0.813–0.941)]. Using optimal cut-off value at 220.94 according to Youden index, the sensitivity was 75.9%, specificity 88.6%, positive likelihood ratio 6.681, negative likelihood ratio 0.272 and accuracy 82.3%. The relative enhancement patterns of benign and malignant lesions, showing 29.92 *vs* 73.08% in the elevated pattern, 7.14 *vs* 92.86% in the steady pattern, 5.71 *vs* 94.29% in the depressed pattern, and 80.00 *vs* 20.00% in non-enhanced lesions ($p < 0.0001$), respectively.
Conclusion: Despite variations in the degree of tumour angiogenesis, quantitative analysis of the breast lesions on CESM documented the malignancies had distinctive stronger enhancement and depressed relative enhancement patterns than benign lesions.
Advances in knowledge: To our knowledge, this is the first study evaluating the feasibility of quantifying lesion enhancement on CESM. The quantities of enhancement were informative for assessing breast lesions in which the malignancies had stronger enhancement and more relative depressed enhancement than the benign lesions.

INTRODUCTION

Mammography remains an important breast-imaging technique for both screening and diagnostic purposes, although the variable density of breast tissue can influence the sensitivity and increase the susceptibility of breast cancer.[1,2] Recently, technical advances in digital imaging have facilitated the development of advanced mammographic imaging techniques including tomosynthesis and dual energy contrast-enhanced spectral mammography (CESM). These modalities have been found to improve the cancer detection rate by resolving the superimposition of breast tissue on conventional mammography in tomosynthesis[3] or enhancing cancers secondary to tumour angiogenesis in CESM.[4–9] While tomosynthesis is suited for breast cancer detection, CESM is preferable for differentiating cancers from benign lesions. The characterisation of breast lesions in these two techniques is crucial for prompt and effective patient management.

CESM can provide low-energy mammograms and additional contrast-enhanced subtracted mammograms within the same examination. The low-energy mammogram has been proven to be qualitatively equivalent to conventional mammograms.[10–12] Under the suppressed background of normal breast tissue, breast cancers characterized by hyperangiogenesis can easily be displayed on CESM due to the presence of iodine uptake. This result indicates the increased possibility of malignancy rather than non-malignancy. However, 6–28% of enhanced lesions have also been documented in certain precancerous or benign diseases[4–7] including atypical ductal hyperplasia, flat epithelial atypia, intraductal papilloma, fibroadenoma, hamartoma, radial scar, or adenosis.[4–7] Furthermore, additional information of associate enhancement could help to assess the probably malignant microcalcifications.[5] In order to better understand the differentiation capability of CESM, we

retrospectively analyzed the quantitative measurement and relative enhancement at early and late phases among pathologically proven benign and malignant lesions. To our knowledge, the feasibility of quantifying lesion enhancement on CESM has not been reported before.

METHODS AND MATERIALS

Patient population and imaging protocol

Approval for this study was obtained from Chang Gung Memorial Hospital's Institutional Review Board. We retrospectively reviewed the cases that had undergone CESM from January 2012 to December 2015 in our hospital. The inclusion criteria were: (1) suspicious malignant breast lesions determined either by mammography or sonography; (2) breast lesions pathologically proven either by image-guided biopsy or surgery; (3) cases where CESM was performed according to our standardized protocol: performing craniocaudal (CC) views first and mediolateral oblique (MLO) views later to quantify the difference of enhancement for the same lesion; and (4) lesions with a clinical follow up of at least 1 year. One male patient was excluded due to the indigenous difficulty of obtaining adequate CC view image on man.

CESM was performed using a commercial mammography apparatus (Senographe Essential CESM; GE Healthcare, Buc, France) using molybdenum or rhodium with automatic cooperation of copper filter. A single-bolus injection of a non-ionic contrast medium (Omnipaque 350 mg I ml^{-1}; GE Healthcare, Dublin, Ireland) was administered, with injection rate of 3 ml s^{-1}, followed by saline chase via an intravenous catheter that was inserted into the forearm prior to the examination. To successfully recombine the image for subtraction, the patients received repeated exposure from low and high energy in 1 to 2 s alterations during each breast-compressed position, resulting in two images below and above the iodine k-edge at 33.2 keV. Image subtractions can be obtained by diminishing the attenuation differences between the low- and high-energy images and reduction of the noise of non-enhancing image. Enhancement secondary to the iodine uptake was measured by the residual net attenuation.

All mammogram acquisitions were sequentially performed with breast holding during imaging. The bilateral breasts compressed in the CC view were first performed, followed by the MLO view. The imaging procedure takes about 2 to 6 min. Due to the longer positioning time of the MLO view compared to the CC view, we designed the acquisition order such that the CC view was performed first, followed by the MLO view. This was to allow post-contrast CC views of the bilateral breasts to be completed within 3 min after the injection of the contrast medium, while the post-contrast MLO views could be accomplished within 6 min after contrast medium injection. The average time interval between the CC and MLO views of our series was 102 s (range from 72 to 156 s). Low- and high-energy acquisitions were almost simultaneously captured during each single view study and then recombined to obtain a subtracted mammogram. Therefore, the imaging procedure provided a total of eight mammography images, including the low-energy image, used as a substitute to the conventional mammogram, and the CESM images.

Imaging analysis

All enhanced breast lesions, including masses, architectural distortions and microcalcifications, were processed using a semi-automatic segmentation programme in MATLAB R2014a (MathWorks, Natick, MA). Semi-automatic segmentation was performed by automatic selection of the region of interest (ROI) of the breast lesions, followed by manually adjustment by a single radiologist with 3 years of experience in breast imaging. The algorithm is mainly based on edge-based segmentation to delineate the contour of breast lesions. This method process included ameliorating the image quality, obtaining energy texture image and detecting the edges,[13] followed by manual correction of the region of interest of the enhanced lesions manually with a free-hand dragging tool. Lesion without identifiable enhancement from both the automatic segmentation and the radiologist was defined as non-enhanced lesions.

The pixel values of enhanced lesions were determined by the semi-automatic segmentation described in the Supplementary Material 1 (Supplementary material available online). After applying volume of interest LUT transformation using non-linear sigmoid function, the pixel values were obtained. The basic equation sigmoid volume of interest look-up table transformation of window centre and window width is $\bar{I}(x,y) = \frac{\text{output range}}{1+e^{\left[-4\frac{I(x,y)-Wc}{Ww}\right]}}$. The descriptive statistics of enhanced lesions was calculated using the maximum, 95th percentile, 75th percentile, mean, skewness, and kurtosis. The enhancement values from either the CC or MLO views were used for analysis. We measured the pixel values from the bounded lesions that were not affected from the shape of lesions. Since we could not separately obtain the exact pixel values of the normal glandular tissue superimposed over the enhanced lesions, the results of enhancement were simply based on the bounded lesions. Otherwise, the enhancement pattern was evaluated at two relative points between the early phase (2 min after the injection of the contrast medium on CC views) and delayed phase (4 min after contrast medium injection on MLO views) of enhancement, respectively. Unlike dynamic contrast-enhanced MRI (DCE-MRI), the relative enhancement on CESM was not ever published previously. In our report, we grouped in three patterns including: (1) elevated pattern (the enhancement increased more than 10% from the early phase to the late phase), (2) steady pattern (the enhancement changed within 10%), and (3) depressed pattern (the enhancement decreased more than 10%) (Figure 1).

Colour-coded map was used for visual demonstration of the enhancement pattern of the same lesion. On the colour-coded map, the reference for colour-coding was based on the average pixel of the whole breast on CESM. Generally, the average pixel had a baseline of zero. A net pixel value greater than the average pixel was counted as a positive value, with all pixel values below the average recorded were counted as zero. The background was set to black and the cancers increased brightness with the net pixel valves. Pixel values below the average pixel of the whole breast were coloured blue as a baseline, and the maximum pixel of the whole image was coloured red using a jet colour-coded map; the sequence used was red, yellow, green, cyan, and blue (colour figures were provided on online version only).

Figure 1. Relative enhancement patterns of early and late phases. Elevated pattern: the interval enhancement increased more than 10%. Steady pattern: the interval enhancement changed within 10%. Depressed pattern: the interval enhancement decreased more than 10%.

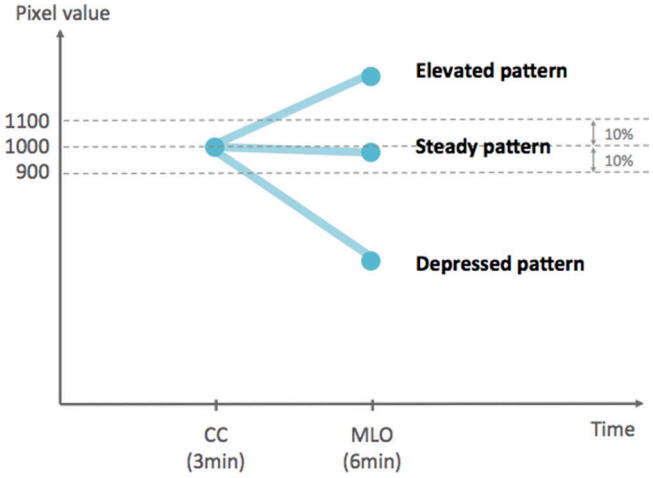

Statistical analysis

The diagnostic accuracy of CESM in the discrimination of benign and malignant lesions was statistically analyzed by Pearson's X^2 test, logistic regression analysis, and receiver operating characteristic (ROC) curve analysis. The best cut-off value was determined using the Youden index, with $Y = sensitivity$ (1 specificity). The sensitivity, specificity, positive likelihood ratio, negative likelihood ratio, and accuracy were then calculated. A p-value < 0.001 was considered to indicate statistical significance. All statistical analyses were performed using the SPSS statistical software (IBM Corp., Armonk, NY).

RESULTS

A total of 152 breast lesions fulfilled the study criteria and were included in the analysis. Of these, all were presented in females, with a mean age of 48.01 years (range, 25–84 years). Of the 152 lesions, 108 were malignancies and 44 were benignities (Table 1).

Table 1. Patient pathological characteristics

Malignant (n = 108)		Benign (n = 44)	
Ductal carcinoma *in situ*	24	Flat epithelial atypia	22
Invasive ductal carcinoma	74	Proliferative breast disease[a]	7
Invasive lobular carcinoma	3	Intraductal papilloma	2
Squamous cell carcinoma	2	Fibroadenoma	5
Metastatic serous adenoma	1	Adenosis	5
Mucinous carcinoma	1	Fibrosis	1
Angiosarcoma	1	Non-proliferative breast disease[b]	2
Adenoid cystic carcinoma	1		
Liposarcoma	1		

[a]Proliferative breast disease other than FEA.
[b]Non-proliferative breast disease other than fibroadenoma, adenosis, fibrosis

After applying semi-automatic segmentation to CESM, there were 104 mass lesions (98 of which enhanced), 44 microcalcifications (10 of which enhanced) and 4 architectural distortions (all of which enhanced). Of all the 152 lesions, 100 of the 108 malignancies (92.59%) and 12 of the 44 non-malignancies (27.27%) exhibited enhancement, while 8 (7.4%) of the malignant lesions and 32 (72.73%) of the non-malignant lesions did not observed enhancement. The eight non-enhancing malignancies all presented with microcalcification only were diagnosed to ductal carcinoma *in situ* (DCIS) in seven (87.5%) and invasive ductal carcinoma (IDC) in one (12.5%). Of these seven DCIS, three were low grade and four were intermediate grade. The only one IDC was Grade 2.

All enhanced lesions were identified and processed using the semi-automatic segmentation programme mentioned above. The non-enhanced lesions were counted as zero. The degree of enhancement was statistically higher in malignancies than in benign diseases in terms of the mean, 75th percentile, 95th percentile, and the maximum (Table 2). The ROC curve revealed good differentiation between malignancies and non-malignancies, and the area under the ROC curve (AUC) was 0.875 [95% confidence interval (CI) 0.811–0.940, p < 0.0001]. The optimal cut-off value was 220.94 according to the Youden index, with a sensitivity of 75.5%, specificity of 88.6%, positive likelihood ratio of 6.642, negative likelihood ratio 0.277, and accuracy of 82.1% (Table 3). Compared to human observers in our study, 24 of 44 benign lesions were initially categorized into Breast Imaging Reporting and Data System 4 due to presence of enhancement. 5 of 24 (20.8%) benign lesions had enhancement degree greater than the optimal cut-off value of 220.94, which indicates the possibility of false positive. In the contrary, 4 DCIS of 108 malignant lesions without enhancement were initially categorized into Breast Imaging Reporting and Data System 2 or 3. However, only one of four (25%) malignant lesions had enhancement greater than 220.94.

There were two lesions only identified on MLO view, therefore two lesions were excluded in the enhancement pattern study. Of the 150 lesions, 106 were malignancies and 44 were benignity. Among the enhancement patterns, the incidence of benign disease and malignancy, respectively, was 26.92% (7/26) and 73.08% (19/26) in the elevated pattern, 7.14% (1/14) and 92.86% (13/14) in the steady pattern, 5.71% (4/70) and 94.29% (66/70) in the depressed pattern, and 80.00% (8/40) and 20.0% (32/40) in non-enhanced lesions. Of the 106 malignant lesions, 62.26% were depressed (Figure 2), 17.92% were elevated (Figure 3), 12.26% were steady (Figure 4), and 7.55% were indeterminate due to non-enhancement (Table 4). The enhancement pattern was found to be statistically significant between the benign and malignant lesions (p < 0.0001).

We separately exploited the CC views (at early phase) and MLO views (at late phase) to evaluate the relative contrast enhancement patterns. In considering to the different degree of compression

Table 2. Enhancement degree: malignant *vs* benign tumours

	Benign	Malignant	*p*-value	OR	95% CI
Mean	85.79	476.05	<0.0001[a]	1.008	1.005–1.010
75th percentile	114.74	588.78	<0.0001[a]	1.006	1.004–1.008
95th percentile	159.72	744.57	<0.0001[a]	1.005	1.003–1.006
Maximum	261.25	1022.20	<0.0001[a]	1.003	1.002–1.004
Kurtosis	1.46	2.99	<0.0001[a]	1.717	1.317–2.237
Skewness	0.11	0.17	0.487	0.457	0.504–4.217

95% CI, 95% confidence interval; OR, odds ratio.
The table illustrates the degree of enhancement of both malignant and benign lesions, including the mean, 75th percentile, 95th percentile, maximum, kurtosis, and skewness. The *p*-value was determined by logistic regression.
[a]A *p*-value < 0.001 is considered to be statistically significant.

and force in the individual positioning, we recorded the breast thickness and compression force of our all cases. The average breast thickness of CC and MLO view of right and left breasts were 52.72, 53.87, 53.41, 53.69 mm and the average compression forces were 135.92 , 142.43, 140.53 and 142.43 Newtons respectively. We believed that the standard requirement for quality control acquired steady pressure and breast thickness that had been published by O'Leary's study.[14] Additionally, the correlation coefficient (intraclass correlation coefficient) of breast thicknesses on the CC view to MLO view of right breast was 0.963 [95% CI (0.948–0.973)] and 0.963 for left breast [95% CI (0.950–0.973)], indicating the excellent consistency. The Bland–Altman plot is shown in Figure 5a,b.

DISCUSSION

CESM is a recently developed breast imaging technique that facilitates the detection and size measurement of cancer by mammographic morphology and angiogenic enhancement. Technical and clinical experiences of CESM have been published elsewhere.[6,7] Many blinded interobserver studies have reported that CESM can improve the diagnosis of breast cancer with increased sensitivity, specificity, positive-predictive value, negative-predictive value, and accuracy.[12,15,16] Otherwise, CESM can assist clinical decision making by identifying potential multifocal, multicentric or bilateral breast cancer before surgery, leading to a change treatment strategy in 19% patients after detection of additional malignant lesions.[17] Our study showed similar findings in which among the 152 breast lesions in 141 patients (11 patients with bilateral lateral lesions), showing 7 of the 108 malignancies and 4 of the 44 non-malignancies.

Table 3. Areas under receiver operating characteristic curve of the degree of enhancement

	AUC	*p*-value	95% CI
Mean	0.877	<0.0001[a]	0.813–0.941
75th percentile	0.877	<0.0001[a]	0.813–0.941
95th percentile	0.875	<0.0001[a]	0.810–0.940
Maximum	0.858	<0.0001[a]	0.787–0.929
Skewness	0.691	<0.0001[a]	0.597–0.785
Kurtosis	0.784	<0.0001[a]	0.687–0.881

95% CI, 95% confidence interval; AUC, area under the curve; Q75, 75 percentile; Q95, 95 percentile; ROC, receiver operating characteristic curve; 95% CI, 95% confidence interval.
The ROC curves of the degree of enhancement including the mean, 75th percentile, 95th percentile, and maximum.
[a]A *p*-valve <0.001 is considered to be statistically significant.

The enhancement technique is an important way of displaying angiogenic lesions. Malignant lesions are mostly hypervascular with immature tumour vessels. As shown in our results, the degree of enhancement of malignant tumours is frequently greater than that of benign lesions. The additional information gained via this method is important for diagnostic consideration. The optimal cut-off value of malignant lesions was calculated to prove the power of the test, although the value was not applied to all cases universally. From our results, we found out that using a cut-off value of 220.94, we can yield a positive likelihood ratio of 6.642, indicating that higher enhancement probably relates to malignancy.

As for other related diagnostic tools, both CESM and DCE-MRI can evaluate suspicious breast lesions using kinetic enhancement. Although CESM has lower sensitivity but better specificity than DCE-MRI, both CESM and DCE-MRI are superior to mammography, especially in dense breast.[18] DCE-MRI is a sensitive imaging modality for the detection of cancer and the interpretation of lesions.[19,20] The continuous acquisition of the enhancement of lesions provides kinetic information for cancer diagnosis with documented diagnostic value.[21] The DCE-MRI lexicon of enhancement curves has been classified into three types according to the change in their signal intensity over time after the injection of a contrast medium, and include persistent enhancement (Type I), plateau (Type II), and washout (Type III) patterns.[21] Kuhl et al[21] reported 101 malignant lesions distributed as follows: Type I, 8.9%; Type II, 33.6%; and Type III, 57.4%. They also reported 165 benign lesions distributed as follows: Type I, 83.0%; Type II, 11.5%; and Type III, 5.5%. These results had an overall diagnostic accuracy of 86.0%, sensitivity of 91.0%, and specificity of 83.0%. Meanwhile, uncertainty remains as to whether iodine would play a role in CESM similar to that of gadolinium in DCE-MRI. Nevertheless, the main concern is the radiation dose administered during the treatment time in order to obtain a continuous time-enhancement curve.

Figure 2. Case of depressed relative enhancement of a 61-year-old female with pathologically proven right breast invasive ductal carcinoma. Mammography CC (a) and MLO views (b) of the right breast revealed a mass lesion in the upper outer quadrant. Colour-coded map CC (c) and MLO views (d) of the right breast revealed depressed relative enhancement. CC, craniocaudal; MLO, mediolateral oblique.

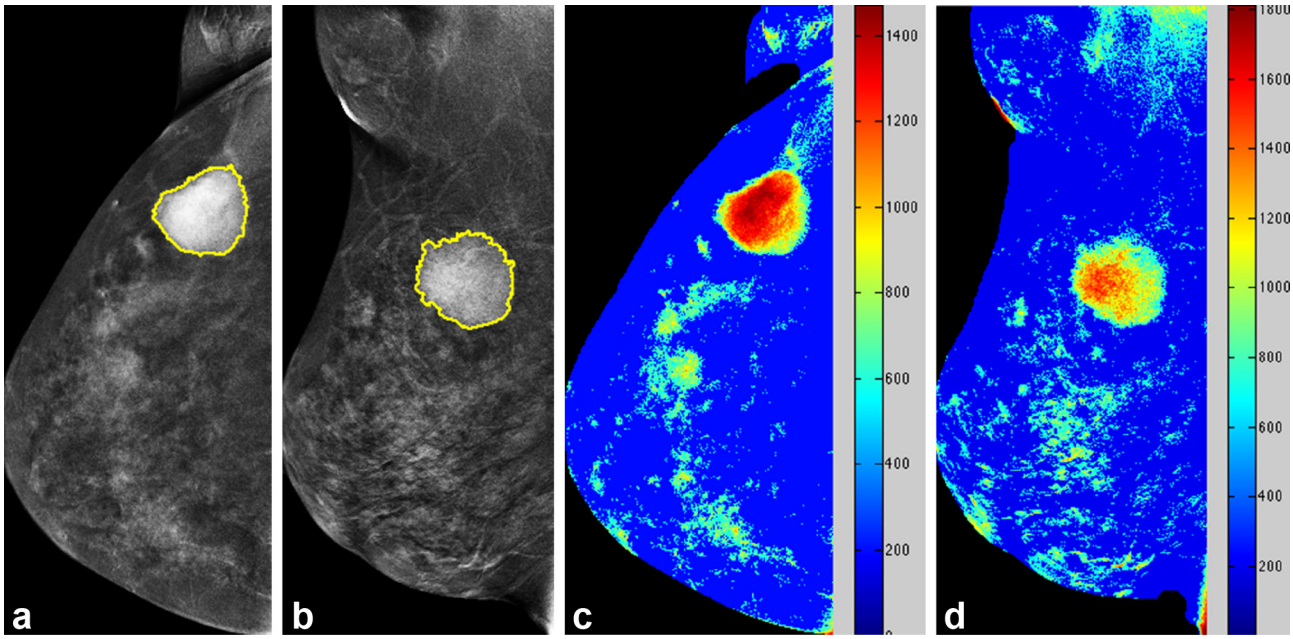

Figure 3. Case of elevated relative enhancement of a 39-year-old female with pathologically proven right breast invasive ductal carcinoma. Mammography CC (a) and MLO views (b) of the right breast revealed a speculated mass lesion in the lower outer quadrant. Colour-coded map CC (c) and MLO views (d) of the right breast revealed elevated relative enhancement. CC, craniocaudal; MLO, mediolateraloblique.

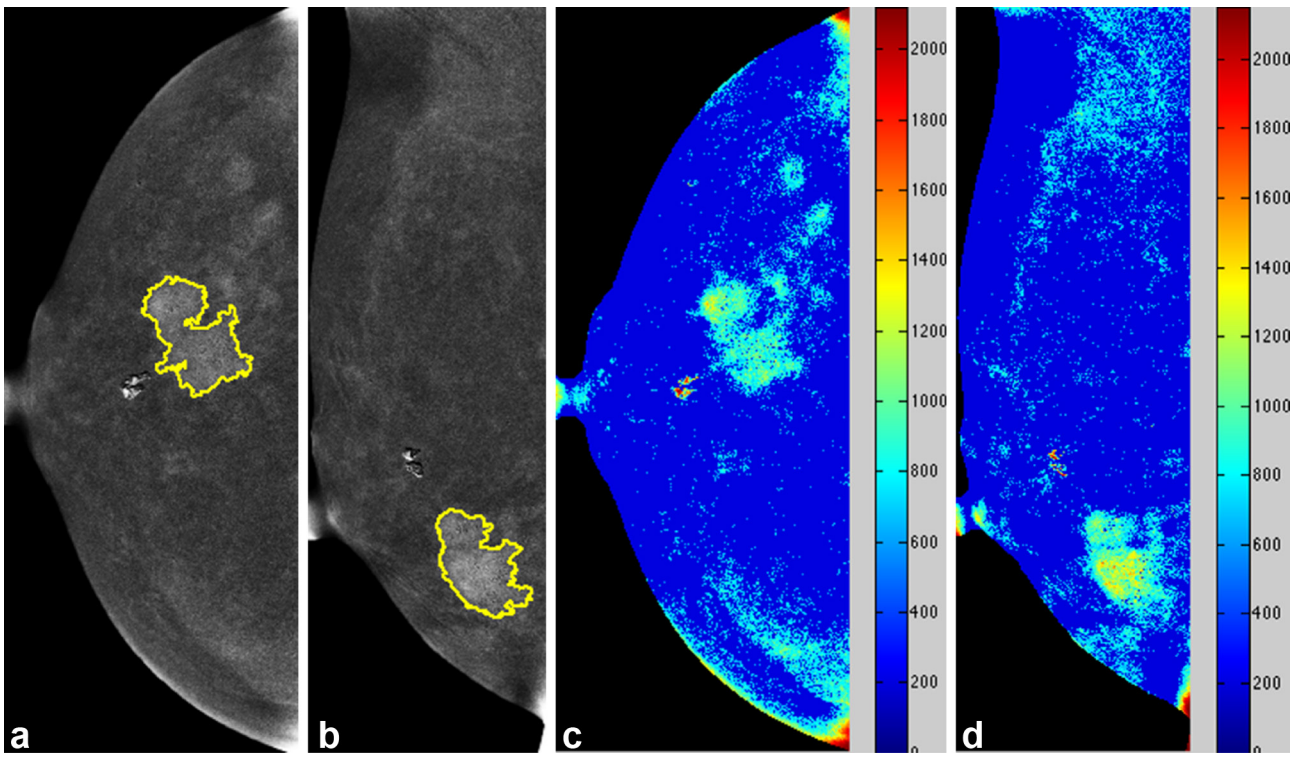

Figure 4. Case of steady relative enhancement of a 39-year-old female with pathologically proven left breast invasive ductal carcinoma. Mammography CC (a) and MLO views (b) of the left breast revealed a strongly enhanced mass lesion in the upper outer quadrant. Colour-coded map CC (c) and MLO views (d) of the right breast revealed steady relative enhancement. CC, craniocaudal; MLO, mediolateral oblique.

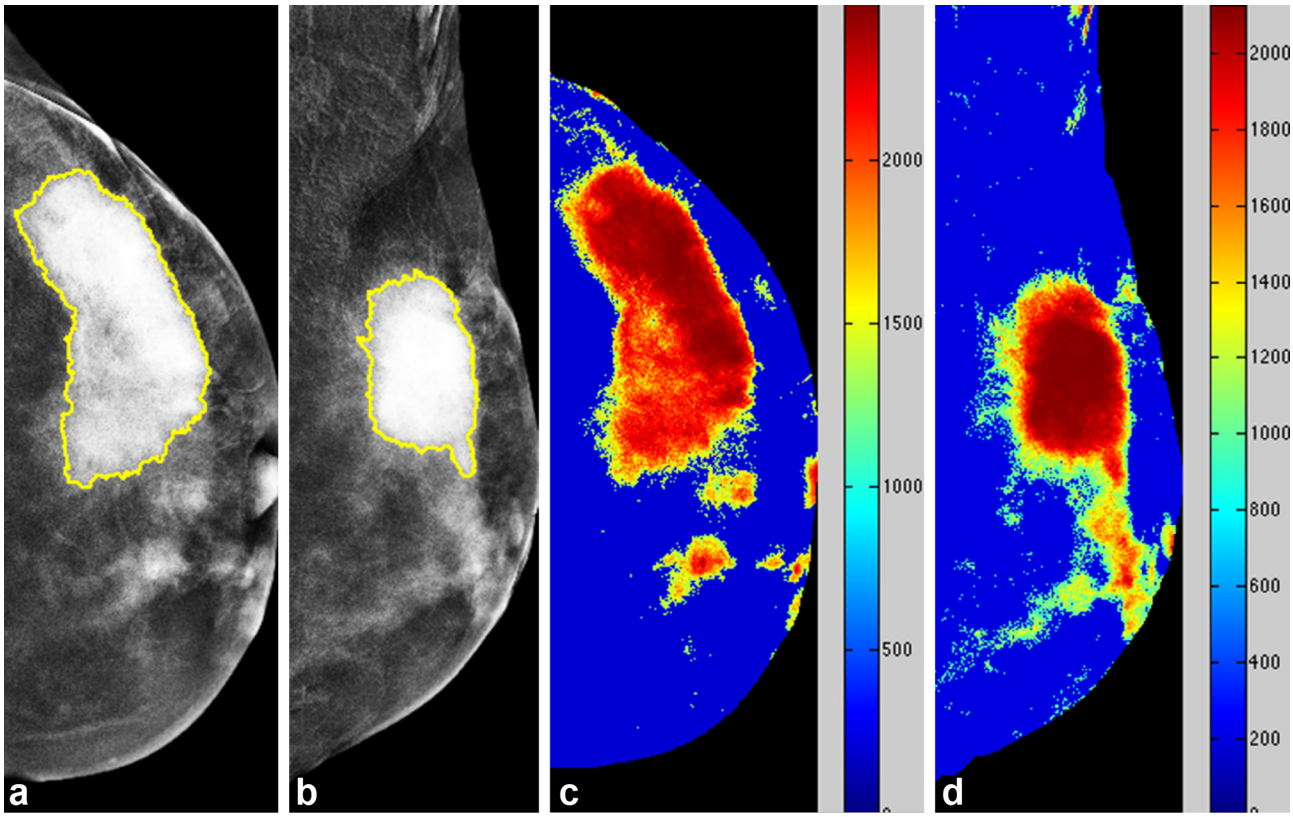

In the past, digital subtraction angiography revealed that the majority of breast cancers had rapid and strong enhancement with washout due to their hypervascularities.[22–24] However, digital subtraction angiography is seldom used due to the invasive nature of the procedure. Similar to breast DCE-MRI, the investigation of tumour enhancement secondary to leakage of the contrast medium into the interstitial spaces is a topic of interest. To our best knowledge, there was no similar CESM report to investigate the enhancement patterns of cancers as compared to our study. Only a CESM study with a different protocol of performance using sequential exposure at 3rd, 5th, 7th and 10th minutes after contrast injection in single to analyze the enhancement patterns of cancers. Their few cases revealed that 3 of 10 (30%) malignant lesions with decreased pattern, 4 of 10 (40%) with plateau pattern, 1 of 10 (10%) with increased pattern and 2 of 10 (20%) without enhancement.[25] A recent advanced study demonstrated a significant correlation of kinetic curves between DCE-MRI with gadolinium and contrast-enhanced digital breast tomosynthesis with iodine.[26] These results indicated that iodine might display enhancement comparable to that of gadolinium

Table 4. Relative early and late enhancements of malignant and benign breast lesions

	Benign (n = 44)	Malignant (n = 106)	Total (n = 150)
Age	49 (33–84)	47.8 (25–73)	47.9 (25–84)
Dynamic kinetic curve			
Elevated	7 (15.91%)	19 (17.92%)	26
Steady	1 (2.27%)	13 (12.26%)	14
Depressed	4 (9.09%)	66 (62.26%)	70
Non-enhanced	32 (72.73%)	8 (7.55%)	40

Pearson's chi-squared test $X^2(3) = 223.972$, $p < 0.0001$.

Figure 5. Bland–Altman plot of breast thickness of bilateral breasts. (a) Bland–Altman plot of breast thickness of right CC view and MLO view. (b) Bland–Altman plot of breast thickness of left CC view and MLO view. CC, craniocaudal; MLO, mediolateralb oblique.

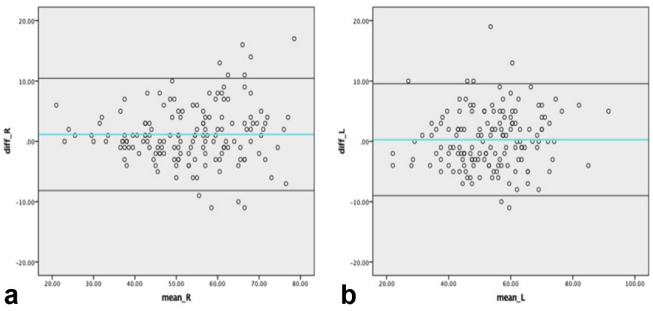

in DCE-MRI. Unfortunately, a high dose of multiexposure radiation was needed to trace the degree of lesion enhancement at subsequent time points in order to plot an enhancement curve.

In contrast to the previous study, we utilized the time interval between the CC views and MLO views to estimate the contrast enhancement characteristics of breast lesions and quantitatively analyze pathologically proven breast lesions using original CESM images. The plotting of enhancement curves requires at least three different time points from DCE-MRI. Additional exposures would, therefore, be in excess of the normal performance of CESM. From our designed analysis using the two image acquisition time points, the relative enhancement at early (CC view) and late (MLO view) net enhancements on CESM is adequate to classify the enhancement as elevated, steady, or depressed.

With regard to DEC-MRI, malignancies typically exhibit maximal enhancement within 2–3 min after the injection of gadolinium either with or without washout. In Kuhl's DCE-MRI study, washout was observed in 57.4% of malignancies.[21] In our CESM study, depressed, steady, and elevated enhancement patterns may correspond to the washout, plateau, and persistent rising enhancement patterns of DCE-MRI, respectively. Approximately, 62.26% of our malignant lesions (66 of 106) exhibited depressed relative enhancements, similar to the washout curve of DCE-MRI by Kuhl's study (57.4%) However, up to 17.92% (19 of 106) of malignant lesions had elevated enhancement that might overlap with benign lesions.

There are several limitations in our study. First, this study was a retrospective analysis on the clinical cases that was performed sequentially with CC views first followed by MLO views for examining bilateral breasts in a same session. We could only document the relative enhancement between early and late phases rather than dynamic kinetic enhancement. Second, CESM was not routinely performed for all cases of malignancy because it is not currently a compulsory modality for clinical management. However, our analyzed cases were consecutively performed without specific histological selection. Third, the thickness of a large breast might delay image acquisitions by more than 6 min after contrast medium injection due to the expenditure of a greater amount of energy. Fortunately, we noticed no such case in our series. Fourth, the reference for the enhancement measurements was based on the average enhancement of the whole breast including normal and abnormal enhancements. This might induce a technical error whereby mild enhanced lesions are masked on the colour-coded map. In our study, seven DCIS and one IDC were observed to have subtle enhancement on the original CESM, but were invisible on the colour-coded map. A correlation with the original CESM could resolve this pitfall. Fifth, the shape and density of the lesions in different views might influence the enhancement results. However, we assume that this effect was limited due to the residual iodine concentration only after the subtraction of high-to-low-energy mammograms.

CONCLUSION

Despite variations in the degree of tumoral angiogenesis, quantitative analysis of the breast lesions on CESM documented distinctive enhancement and relative enhancement patterns among the malignant and benign lesions.

REFERENCES

1. Cheung YC, Lin YC, Wan YL, Yeow KM, Huang PC, Lo YF, et al. Diagnostic performance of dual-energy contrast-enhanced subtracted mammography in dense breasts compared to mammography alone: interobserver blind-reading analysis. *Eur Radiol* 2014; **24**: 2394–403. doi: https://doi.org/10.1007/s00330-014-3271-1
2. Boyd NF, Martin LJ, Bronskill M, Yaffe MJ, Duric N, Minkin S. Breast tissue composition and susceptibility to breast cancer. *J Natl Cancer Inst* 2010; **102**: 1224–37. doi: https://doi.org/10.1093/jnci/djq239
3. Kopans DB. Digital breast tomosynthesis from concept to clinical care. *AJR Am J Roentgenol* 2014; **202**: 299–308. doi: https://doi.org/10.2214/AJR.13.11520
4. Lewin JM, Isaacs PK, Vance V, Larke FJ. Dual-energy contrast-enhanced digital subtraction mammography: feasibility. *Radiology* 2003; **229**: 261–8. doi: https://doi.org/10.1148/radiol.2291021276
5. Cheung YC, Tsai HP, Lo YF, Ueng SH, Huang PC, Chen SC. Clinical utility of dual-energy contrast-enhanced spectral mammography for breast microcalcifications without associated mass: a preliminary analysis. *Eur Radiol* 2016; **26**: 1082–9. doi: https://doi.org/10.1007/s00330-015-3904-z
6. Dromain C, Thibault F, Diekmann F, Fallenberg EM, Jong RA, Koomen M, et al. Dual-energy contrast-enhanced digital mammography: initial clinical results of a multireader, multicase study. *Breast Cancer Res* 2012; **14**: R94. doi: https://doi.org/10.1186/bcr3210
7. Dromain C, Thibault F, Muller S, Rimareix F, Delaloge S, Tardivon A, et al. Dual-energy contrast-enhanced digital mammography: initial clinical results. *Eur Radiol* 2011; **21**: 565–74. doi: https://doi.org/10.1007/s00330-010-1944-y
8. Dromain C, Balleyguier C, Muller S, Mathieu MC, Rochard F, Opolon P, et al. Evaluation of tumor angiogenesis of breast carcinoma using contrast-enhanced digital mammography. *AJR Am J Roentgenol* 2006; **187**: W528–W537. doi: https://doi.org/10.2214/AJR.05.1944
9. Diekmann F, Diekmann S, Jeunehomme F, Muller S, Hamm B, Bick U. Digital mammography using iodine-based contrast media. *Invest Radiol* 2005; **40**: 397–404. doi: https://doi.org/10.1097/01.rli.0000167421.83203.4e
10. Francescone MA, Jochelson MS, Dershaw DD, Sung JS, Hughes MC, Zheng J, et al. Low energy mammogram obtained in contrast-enhanced digital mammography (CEDM) is comparable to routine full-field digital mammography (FFDM). *Eur J Radiol* 2014; **83**: 1350–5. doi: https://doi.org/10.1016/j.ejrad.2014.05.015
11. Lalji UC, Jeukens CR, Houben I, Nelemans PJ, van Engen RE, van Wylick E, et al. Evaluation of low-energy contrast-enhanced spectral mammography images by comparing them to full-field digital

mammography using EUREF image quality criteria. *Eur Radiol* 2015; **25**: 2813–20. doi: https://doi.org/10.1007/s00330-015-3695-2
12. Luczyńska E, Heinze-Paluchowska S, Dyczek S, Blecharz P, Rys J, Reinfuss M. Contrast-enhanced spectral mammography: comparison with conventional mammography and histopathology in 152 women. *Korean J Radiol* 2014; **15**: 689–96. doi: https://doi.org/10.3348/kjr.2014.15.6.689
13. Zhang Y, Tomuro N, Furst J, Stan Raicu D. Image enhancement and edge-based mass segmentation in mammogram. In: Dawant BM, Haynor DR, eds. *Medical imaging 2010: image processing*. **vol. 7623**. San Diego, CL, USA: SPIE; 2010. pp. 72634.
14. O'Leary D, Grant T, Rainford L. Image quality and compression force: the forgotten link in optimisation of digital mammography? *Breast Cancer Research* 2011; **13**(Suppl 1): P10. doi: https://doi.org/10.1186/bcr2962
15. Blum KS, Antoch G, Mohrmann S, Obenauer S. Use of low-energy contrast-enhanced spectral mammography (CESM) as diagnostic mammography-proof of concept. *Radiography* 2015; **21**: 352–8. doi: https://doi.org/10.1016/j.radi.2015.02.005
16. Wang Q, Li K, Wang L, Zhang J, Zhou Z, Feng Y. Preclinical study of diagnostic performances of contrast-enhanced spectral mammography versus MRI for breast diseases in China. *Springerplus* 2016; **5**: 763. doi: https://doi.org/10.1186/s40064-016-2385-0
17. Tardivel AM, Balleyguier C, Dunant A, Delaloge S, Mazouni C, Mathieu MC, et al. Added value of contrast-enhanced spectral mammography in postscreening assessment. *Breast J* 2016; **22**: 520–8. doi: https://doi.org/10.1111/tbj.12627
18. Fallenberg EM, Schmitzberger FF, Amer H, Ingold-Heppner B, Balleyguier C, Diekmann F, et al. Contrast-enhanced spectral mammography vs. mammography and MRI – clinical performance in a multi-reader evaluation. *Eur Radiol* 2017; **27**: 2752–64. doi: https://doi.org/10.1007/s00330-016-4650-6
19. Kuhl C. The current status of breast MR imaging. Part I. Choice of technique, image interpretation, diagnostic accuracy, and transfer to clinical practice. *Radiology* 2007; **244**: 356–78. doi: https://doi.org/10.1148/radiol.2442051620
20. Kuhl CK. Current status of breast MR imaging. Part 2. Clinical applications. *Radiology* 2007; **244**: 672–91. doi: https://doi.org/10.1148/radiol.2443051661
21. Kuhl CK, Mielcareck P, Klaschik S, Leutner C, Wardelmann E, Gieseke J, et al. Dynamic breast MR imaging: are signal intensity time course data useful for differential diagnosis of enhancing lesions? *Radiology* 1999; **211**: 101–10. doi: https://doi.org/10.1148/radiology.211.1.r99ap38101
22. Watt AC, Ackerman LV, Windham JP, Shetty PC, Burke MW, Flynn MJ, et al. Breast lesions: differential diagnosis using digital subtraction angiography. *Radiology* 1986; **159**: 39–42. doi: https://doi.org/10.1148/radiology.159.1.3513251
23. Ackerman LV, Watt AC, Shetty P, Flynn MJ, Burke M, Kambouris A, et al. Breast lesions examined by digital angiography. Work in progress. *Radiology* 1985; **155**: 65–8. doi: https://doi.org/10.1148/radiology.155.1.3883425
24. Watt AC, Ackerman LV, Windham JP, Shetty PC, Burke MW, Flynn MJ, et al. Breast lesions: differential diagnosis using digital subtraction angiography. *Radiology* 1986; **159**: 39–42. doi: https://doi.org/10.1148/radiology.159.1.3513251
25. Jong RA, Yaffe MJ, Skarpathiotakis M, Shumak RS, Danjoux NM, Gunesekara A, et al. Contrast-enhanced digital mammography: initial clinical experience. *Radiology* 2003; **228**: 842–50. doi: https://doi.org/10.1148/radiol.2283020961
26. Froeling V, Diekmann F, Renz DM, Fallenberg EM, Steffen IG, Diekmann S, et al. Correlation of contrast agent kinetics between iodinated contrast-enhanced spectral tomosynthesis and gadolinium-enhanced MRI of breast lesions. *Eur Radiol* 2013; **23**: 1528–36. doi: https://doi.org/10.1007/s00330-012-2742-5